

Mechanism analysis of reaction $S^+(^2D)+H_2(X^1\Sigma_g^+) \rightarrow SH^+(X^3\Sigma^-)+H(^2S)$ based on the quantum state-to-state dynamics

Jin-Yu Zhang(张金玉), Ting Xu(许婷), Zhi-Wei Ge(葛志伟), Juan Zhao(赵娟), Shou-Bao Gao(高守宝), Qing-Tian Meng(孟庆田)

Citation: Chin. Phys. B . 2020, 29(6): 063101 . **doi:** 10.1088/1674-1056/ab889c
Journal homepage: http://cpb.iphy.ac.cn; http://iopscience.iop.org/cpb

What follows is a list of articles you may be interested in

Dynamics of the $Au+H_2$ reaction by time-dependent wave packet and quasi-classical trajectory methods

Yong Zhang(张勇), Chengguo Jiang(姜成果)

Chin. Phys. B . 2019, 28(12): 123101 . **doi:** 10.1088/1674-1056/ab52f2

Reaction mechanism of $D+ND \rightarrow N+D_2$ and its state-to-state quantum dynamics

Ting Xu(许婷), Juan Zhao(赵娟), Xian-Long Wang(王宪龙), Qing-Tian Meng(孟庆田)

Chin. Phys. B . 2019, 28(2): 023102 . **doi:** 10.1088/1674-1056/28/2/023102

State-to-state dynamics of $F(^2P)+HO(^2\Pi) \rightarrow O(^3P)+HF(^1\Sigma^+)$ reaction on $1^3A"$ potential energy surface

Juan Zhao(赵娟), Hui Wu(吴慧), Hai-Bo Sun(孙海波), Li-Fei Wang(王立飞)

Chin. Phys. B . 2018, 27(2): 023102 . **doi:** 10.1088/1674-1056/27/2/023102

State-to-state quantum dynamics of $N(^2D)+HD$ (v=0, j=0) reaction

Yong Zhang(张勇)

Chin. Phys. B . 2016, 25(12): 123104 . **doi:** 10.1088/1674-1056/25/12/123104

State-to-state quantum dynamics of the $N(^4S)+H_2(X^1\Sigma^+) \rightarrow NH(X^3\Sigma^-)+H(^2S)$ reaction and its reaction mechanism analysis

Zhang Jing, Gao Shou-Bao, Wu Hui, Meng Qing-Tian

Chin. Phys. B . 2015, 24(8): 083104 . **doi:** 10.1088/1674-1056/24/8/083104

Mechanism analysis of reaction $S^+(^2D)+H_2(X^1\Sigma_g^+) \rightarrow SH^+(X^3\Sigma^-)+H(^2S)$ based on the quantum state-to-state dynamics*

Jin-Yu Zhang(张金玉)[1], Ting Xu(许婷)[1,†], Zhi-Wei Ge(葛志伟)[1], Juan Zhao(赵娟)[2], Shou-Bao Gao(高守宝)[1,3], and Qing-Tian Meng(孟庆田)[1,‡]

[1] *School of Physics and Electronics, Shandong Normal University, Jinan* 250358, *China*
[2] *School of Science, Shandong Jiaotong University, Jinan* 250357, *China*
[3] *Shandong Provincial Key Laboratory of Biophysics, Institute of Biophysics, Dezhou University, Dezhou* 253023, *China*

(Received 22 March 2020; revised manuscript received 5 April 2020; accepted manuscript online 12 April 2020)

We present a state-to-state dynamical calculation on the reaction $S^+ + H_2 \rightarrow SH^+ + H$ based on an accurate X^2A'' potential surface. Some reaction properties, such as reaction probability, integral cross sections, product distribution, *etc*., are found to be those with characteristics of an indirect reaction. The oscillating structures appearing in reaction probability *versus* collision energy are considered to be the consequence of the deep potential well in the reaction. The comparison of the present total integral cross sections with the previous quasi-classical trajectory results shows that the quantum effect is more important at low collision energies. In addition, the quantum number inversion in the rotational distribution of the product is regarded as the result of the heavy–light–light mass combination, which is not effective for the vibrational excitation. For the collision energies considered, the product differential cross sections of the title reaction are mainly concentrated in the forward and backward regions, which suggests that there is a long-life intermediate complex in the reaction process.

Keywords: state-to-state reaction dynamics, time-dependent wave packet, $S^+ + H_2$, differential and integral cross sections

PACS: 31.15.xv, 34.50.–s, 82.20.Bc **DOI:** 10.1088/1674-1056/ab889c

1. Introduction

Sulfur-containing molecules have attracted great attention because of their importance in chemical engineering and the early atmosphere of the earth.[1–3] Specially, H_2S^+, as the simplest sulfur containing molecular ion, not only is an indispensable reaction intermediate in the combustion process, but also has a relevant role in the formation of molecules. Because of the possible roles in interstellar-cloud chemistry,[4–6] a lot of researches about H_2S^+ have been done over the past years.

Up to now, there have been many works to study the dynamics of the H_2S^+ system. Experimentally, Horani *et al.*[7] observed the original electronic spectra of H_2S^+ in the range of 400 nm–600 nm for the first time by the low energy electron excitation technique. Dixon *et al.*[8] confirmed the above observed spectra coming from the emission of H_2S^+ radical ion and presented the selection rules for the photoelectron spectra. Later, Duxbury *et al.*[9] carried out the further rotational analysis of the electronic emission spectra of H_2S^+, gave the topological natures of $^2B_1$ and $^2A_1$ states, and explained the complicated ro-vibronic structure of the excited states with both Renner effect and spin–orbit interaction. Delwiche *et al.*[10] analyzed the high-resolution photoelectron spectroscopy of H_2S and obtained the ionization energies and frequencies for $^2B_1$, $^2A_1$, and $^2B_2$ states of H_2S^+. Using the mass-analyzed threshold ionization photofragment excitation technique, Han *et al.*[11] studied the rotationally resolved spectroscopy of the $\tilde{A}^2A_1 \leftarrow \tilde{X}^2B_1$ transition of H_2S^+, and found that the further photoexcitation can lead to the $H_2S^+ \rightarrow H_2 + S^+$ dissociation. In 2014, Duxbury *et al.*[6] connected different methods to give a detailed description of the relation among different types of spectroscopy.

Theoretically, using the *ab initio* molecular orbital method, Sakai *et al.*[12] studied the potential curves of H_2S^+ system and described the electronic structure and geometry of H_2S^+. The related potential energy surface (PES) investigation of H_2S^+ system began from Bruna *et al.*,[13] who carried out the electronic structure calculation of states $^2B_1$, $^2A_1$, and $^2B_2$ employing the large-scale configuration–interaction method. Utilizing the coupled electron-pair electronic wave functions, Lahmar *et al.*[14] calculated the spectroscopic parameters, the vibrational band origins and the rotation-resolved infrared absorption spectra of X^2B_1 and A^2A_1 states for H_2S^+. *Ab initio* calculations have been

*Project supported by the National Natural Science Foundation of China (Grant No. 11674198), the Taishan Scholar Project of Shandong Province, China (Grant No. ts201511025), and the Science Fund from the Shandong Provincial Laboratory of Biophysics.

†Corresponding author. E-mail: 1666456849@qq.com
‡Corresponding author. E-mail: qtmeng@sdnu.edu.cn

© 2020 Chinese Physical Society and IOP Publishing Ltd

implemented by Takeshita and Shida[15] to investigate the molecular configurations and the vibrational energy levels of the X^2B_1, A^2A_1, and B^2B_2 states. In 2003, Hirst[16] constructed the PESs of H_2S^+ system for states X^2B_1, A^2A_1, B^2B_2, 1^4A_2, and 1^4B_1 by carrying out the multiple reference configuration–interaction (MRCI) with the cc-pVQZ basis set, and analyzed the conical intersection between A^2A_1 and B^2B_2 states. In 2005, Li and Huang[17] investigated the doublet electronic states of the H_2S^+ ion with the C_s and C_{2v} symmetries, employing the complete active space self-consistent field (CASSCF), multi-configuration second-order perturbation theory (CASPT2) method, and the atomic natural orbital (ANO) basis. Then using the CASSCF and the CASPT2 methods, Chang and Huang[18] explored the photodissociation through the A^2A_1 state, and found that the $1^2A''$ and $1^2A'$ states associate with the $S^+(^2D)+H_2$ limit in the C_s symmetry. Zanchet *et al.*[19] studied the dynamics of the $S^+(^4S)+H_2(X^1\Sigma_g^+)$ reaction on the quartet state X^4A'' of H_2S^+ using the quasi-classical trajectories (QCT) method. Subsequently, Song *et al.*[20] gave a new PES for the X^4A'' state of H_2S^+ and analyzed the dynamics behavior of the $S^+(^4S)+H_2(X^1\Sigma_g^+)\rightarrow SH^+(X^3\Sigma^-)+H(^2S)$ reaction with QCT method.

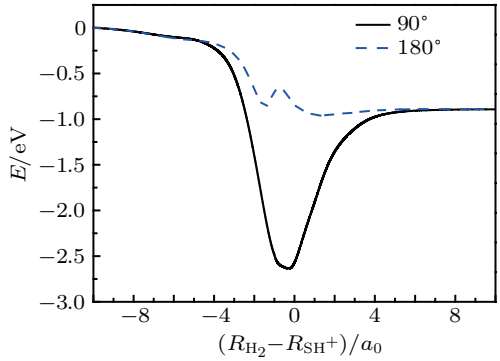


Fig. 1. Minimum energy path for the $S^+(^2D)+H_2(X^1\Sigma_g^+)\rightarrow SH^+(X^3\Sigma^-)+H(^2S)$ reaction as a function $R_{H_2}-R_{SH^+}$ with perpendicular configuration $\angle[SHH]^+=90°$ (solid line) and collinear configuration $\angle[SHH]^+=180°$ (dashed line).

Recently, Zhang *et al.*[21] constructed a novel global PES (hereafter referred to as Zhang PES) for state X^2A'' of H_2S^+ system at first time by the MRCI method containing the Davidson correction. In this work, a switching function has been introduced to remove $S^+(^2D)$ from the dissociation channel of H_2S^+. Then this PES was employed to study the dynamics of $S^+(^2D)+H_2(X^1\Sigma_g^+)\rightarrow SH^+(X^3\Sigma^-)+H(^2S)$ reaction. For the Zhang PES, all *ab initio* energy points were gained utilizing the correlation consistent aug-cc-pVQdZ and aug-cc-pV5dZ orbital basis sets. The minimum energy path (MEP)[22] of title reaction, defined by the potential energy of H_2S^+ as a function of the reaction coordinate $R_{H_2}-R_{SH^+}$, is displayed in Fig. 1. Obviously, in the approaching of S^+ to H_2 perpendicularly, there is a deep well of about 2.653 eV relative to the $S^+ + H_2$ reactant. Besides, the exoergic energy along this MEP is 0.909 eV.

In the present work, we carried out the time-dependent wave packet (TDWP) calculation at the state-to-state level to study the reaction dynamics of $S^+(^2D)+H_2(X^1\Sigma_g^+)\rightarrow SH^+(X^3\Sigma^-)+H(^2S)$ based on Zhang PES[21] in a collision energy range 0.1 eV–1.0 eV and explore its reaction mechanisms. This paper is arranged as follows. In Section 2 we give a briefly outline about the theoretical method of our dynamics calculation. The results and the related discussions are presented in Section 3. And finally, a brief summary is given in Section 4.

2. Method

Since the state-to-state dynamics can present the process of reaction at the microscopic level, it is often used to study the internal mechanism of the related reactions. However, for most state-to-state calculations, the consumption of computing time is a great challenge. In order to resolve this problem, Zhang and Han[23–25] developed a graphics processing units (GPU) version of quantum wave packet program with high parallelism. Besides, this version of TDWP program was later successfully used to investigate the reactions of triatomic systems.[26–34] In this paper, we used this GPU version based on the product coordinate to study the state-to-state chemical dynamics of the reaction $S^+ + H_2 \rightarrow SH^+ + H$.

For the title reaction, the Hamiltonian with the total angular momentum J in the body-fixed (BF) representation can be expressed by

$$\hat{H}=-\frac{\hbar^2}{2\mu_R}\frac{\partial^2}{\partial R^2}-\frac{\hbar^2}{2\mu_r}\frac{\partial^2}{\partial r^2}+\frac{(\hat{J}-\hat{j})^2}{2\mu_R R^2}+\frac{\hat{j}^2}{2\mu_r r^2}+V_{\rm pes} \quad (1)$$

with R being the distance between H atom and the mass center of diatomic molecule SH^+, r the internuclear distance of diatomic molecule SH^+, μ_R and μ_r the reduced masses expressed, respectively, by $\mu_R=m_H(m_{S^+}+m_H)/(m_{S^+}+2m_H)$ and $\mu_r=m_{S^+}m_H/(m_{S^+}+m_H)$. $\hat{J}$ and $\hat{j}$ are, respectively, the total angular momentum operator and the rotational angular momentum operator of SH^+ molecule, $V_{\rm pes}$ is the potential energy of the SH_2^+ system.

Taking the space-fixed (SF) reactant Jacobi coordinates, the initial wave packet can be expressed as

$$|\chi_{\alpha i}\rangle = \left|\Psi^{JM\varepsilon}_{\alpha v_0 j_0 l_0}\right\rangle = |G(R_\alpha)\rangle\left|\phi_{v_0 j_0}(r_\alpha)\right\rangle|JMj_0l_0\varepsilon\rangle\,, \quad (2)$$

where i is the label used for denoting the initial electronic state, α and hereinafter β denotes, respectively, the reactant and product channels. $|G(R_\alpha)\rangle$ and $\left|\phi_{v_0 j_0}(r_\alpha)\right\rangle$ are, respectively, the Gaussian wave packet and the rovibrational eigenfunction for H_2, $|JMj_0l_0\varepsilon\rangle$ the SF rotational basis, and ε the parity given by $\varepsilon=(-1)^{j_0+l_0}$. For convenience to calculate, the wave packet in SF Jacobi coordinates can be converted into one in BF Jacobi coordinates. Using the split-operator scheme,

the propagation of the wave packet in BF product Jacobi coordinates can be realized by[32]

$$\Psi^{JM\varepsilon}(\boldsymbol{R},\boldsymbol{r},t+\Delta) = \mathrm{e}^{-\mathrm{i}\hat{H}_0\Delta/2}\mathrm{e}^{-\mathrm{i}\hat{V}_{\mathrm{rot}}\Delta/2}\mathrm{e}^{-\mathrm{i}V\Delta}\mathrm{e}^{-\mathrm{i}\hat{V}_{\mathrm{rot}}\Delta/2} \times \mathrm{e}^{-\mathrm{i}\hat{H}_0\Delta/2}\Psi^{JM\varepsilon}(\boldsymbol{R},\boldsymbol{r},t), \quad (3)$$

where

$$\hat{H}_0 = -\frac{\hbar^2}{2\mu_R}\frac{\partial^2}{\partial R^2} - \frac{\hbar^2}{2\mu_r}\frac{\partial^2}{\partial r^2} + V_r(r), \quad (4)$$

$$V_{\mathrm{rot}} = \frac{\hat{L}^2}{2\mu_R R^2} + \frac{\hat{j}^2}{2\mu_r r^2}, \quad (5)$$

with $L = J - j$, $V = V_{\mathrm{pes}} - V_r(r)$, $V_r(r)$ being the reference potential of diatomic molecule SH^+.

After the propagation, the radial component of product state wave function is provided by

$$\left|\chi_{\beta\mathrm{f}}\right\rangle = \delta(R_\beta - R_\infty)\left|\phi_{v'j'}(r_\beta)\right\rangle\left|JMj'l'\right\rangle, \quad (6)$$

in which f labels the final state, R_∞ the fixed radial coordinate of the asymptotic region, and $(v'j')$ the final ro-vibrational quantum numbers. Then the scattering matrix element expressed in BF Jacobi coordinates has the form of

$$S_{\mathrm{fi}} = [2\pi a_{\alpha\mathrm{i}}(E)a^*_{\beta\mathrm{f}}(E)]^{-1} \times \int_{-\infty}^{+\infty}\mathrm{d}t\,\mathrm{e}^{(\mathrm{i}/\hbar)Et}\left\langle\chi_{\beta\mathrm{f}}\right|\mathrm{e}^{-(\mathrm{i}/\hbar)\hat{H}t}\left|\chi_{\alpha\mathrm{i}}\right\rangle \quad (7)$$

with the coefficients

$$a_{\alpha\mathrm{i}}(E) = \left\langle\phi_{\mathrm{i}}|\chi^+_{\mathrm{i}}\right\rangle = \left\langle \mathrm{i}\sqrt{\mu_R k_{\alpha\mathrm{i}}/2\pi}R_\alpha \mathrm{h}^{(2)}_{l_\alpha}(k_{\alpha\mathrm{i}}R_\alpha)|G(R_\alpha)\right\rangle, \quad (8)$$

$$a_{\beta\mathrm{f}}(E) = \left\langle\phi_{\mathrm{f}}|\chi^+_{\mathrm{f}}\right\rangle = \left\langle\sqrt{\mu_R k_{\beta\mathrm{f}}/2\pi}R_\beta \mathrm{h}^{(1)}_{l_\beta}(k_{\beta\mathrm{f}}R_\beta)|\delta(R_\beta - R_\infty)\right\rangle, \quad (9)$$

in which $\mathrm{h}^{(1)}$ and $\mathrm{h}^{(2)}$ are, respectively, the first and second kind spherical Hankel functions.

Consequently, the differential cross sections (DCSs) and integral cross sections (ICSs) are expressed as

$$\frac{\mathrm{d}\sigma_{v'j',v_0j_0}(\theta,E)}{\mathrm{d}\Omega} = (2j_0+1)^{-1}\sum_{K'}\sum_{K_0}\left|(2\mathrm{i}k_{v_0j_0})^{-1}\sum_J(2J+1)d^J_{K'K_0}(\theta)S^J_{v'j'K',v_0j_0K_0}\right|^2, \quad (10)$$

$$\sigma_{v'j',v_0j_0} = (2j_0+1)^{-1}k^{-2}_{v_0j_0}\sum_{K'}\sum_{K_0}\sum_J(2J+1)\left|S^J_{v'j'K',v_0j_0K_0}\right|^2, \quad (11)$$

with θ being the scattering angle, $k_{v_0j_0}$ the initial translational wave vector for the reactant, K' and K_0, respectively, the initial and final helicity quantum numbers. $d^J_{K'K_0}(\theta)$ denotes the reduced rotation matrix.

3. Results and discussion

3.1. Numerical aspects

Here we applied the TDWP method to investigate the reaction dynamics of $S^+(^2D) + H_2(X^1\Sigma_g^+) \rightarrow SH^+(X^3\Sigma^-) + H(^2S)$. For the collision energy up to 1.0 eV, the angular momentum J is up to 95, which can give the converged ICSs. In addition, we carried out a series of tests to ensure the parameters are suitable for obtaining the convergent results. The test results are shown in Table 1. The effect of the Coriolis coupling[35] is considered strictly in our calculation. So, for a given J, the reaction probability should include all possible K terms. In fact, since for some large J values, the large K term contributes little to the reaction probability, it is not necessary to calculate all K terms. The convergence test for total angular momentum $J = 60$ is listed in Fig. 2. It can be seen from this figure that the curves, although there are some oscillations in them, do not have a great change in the overall trend. Besides, for a given J, the convergent results can be obtained if we take $K = \min(19, J+1)$.

Table 1. Parameters used in wave-packet propagation (except for the number of arguments, others are in atomic unit).

Parameter	Value
Range of product scatter coordinate R	0.02–20.0
Grid point number in R	180
Translational basis function number in the interaction region	150
Range of product scatter coordinate r	0.5–18.0
Grid point number in r	180
Vibrational basis function number in the interaction region	100
Angular grid point number	160
Initial wave-packet center (R_0)	14.0
Wave-packet width (δ)	0.225
Integration time interval (Δ)	10
Absorption length in R/r	4.0/4.0
Absorption intensity in R/r	0.005/0.005
Flux analysis position in R/r	15.0/13.0
Propagation time	50000

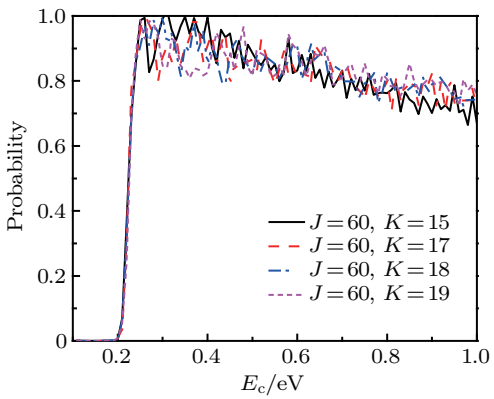


Fig. 2. The reaction probability convergence tests of K for $J = 60$.

3.2. Reaction probabilities and ICSs

The reaction probabilities changing with collision energies at some selected J partial waves are displayed in Fig. 3. Obviously, because of the existence of the potential well, all the curves are with the oscillating features. In addition, since the reaction $S^+ + H_2 \rightarrow SH^+ + H$ is a barrierless and exothermic one, the probability curves with small J values are of no threshold energy. With the increase of J, the reaction threshold begins to appear and tends to the higher energy, which is the result of the centrifugal potential barrier increasing with J value. One interesting phenomenon in this figure is that when J is mall enough to avoid the appearance of the threshold energy, the related maximal reaction probability is enhanced with the increase of J value. However, when J is large enough to lead to the occurrence of the threshold value, the related maximal reaction probability is decreased with increasing J value. This is also the consequence of the centrifugal potential barrier for an exothermic reaction, *i.e.*, after the threshold energy is deducted, the increasing of the residual rotation energy can prohibit the reaction process. Certainly, due to the same reason, the reaction probability decreases gradually with the increase of the collision energy.

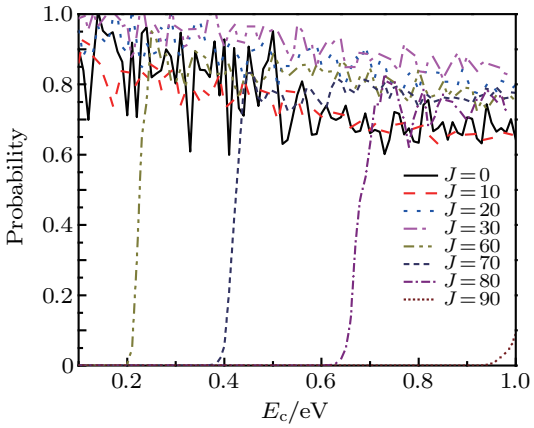


Fig. 3. Total reaction probabilities changing with collision energy for reaction $S^+ + H_2 \rightarrow SH^+ + H$ at some selected J's.

Figure 4 shows the opacity functions of reaction $S^+ + H_2 \rightarrow SH^+ + H$ at selected collision energies. Obviously, because of the existence of a deep potential well in this reaction, the indirect mechanism is dominated, and all the opacity function curves are with abundant oscillations. For the collision energy 0.2 eV, the reaction involves only a small quantity of partial waves, which is because the weaker rotational excitation is arisen by the smaller collision energy. With the collision energy increasing, more partial waves participate in the reaction. For a specific collision energy, the curve rises slowly with the increase of the J, reaches the maximum value at a certain J, and is reduced rapidly to zero with the increase of J value. The larger maximum value of the opacity function corresponds to the larger collision energy. All the curves in Fig. 4 show the similar properties. Therefore, we can speculate that the reaction has a similar reaction mechanism under different collision energies considered.

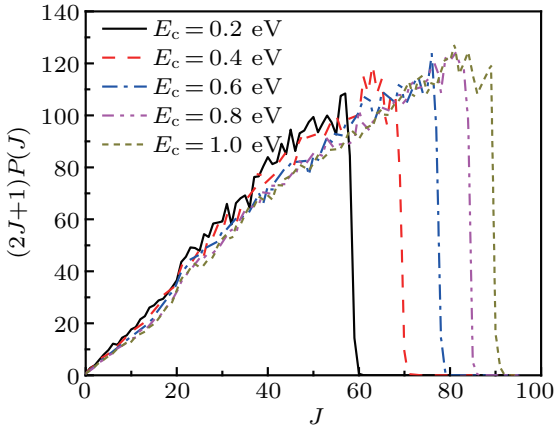


Fig. 4. $(2J+1)$ weighted opacity functions of reaction $S^+ + H_2 \rightarrow SH^+ + H$ at five collision energies.

Figure 5 displays the total ICSs of reaction $S^+ + H_2(v = 0, j = 0) \rightarrow SH^+ + H$ together with the results obtained from QCT method[21] for comparison. On the overall point of view, the curve of the ICS calculated by us agrees well with the QCT result, but at low collision energies, the present work has a slight deviation from the QCT result. This phenomenon can be explained by that in the present state-to-state quantum dynamics, the zero-point-energy (ZPE) is considered naturally, whereas in the previous QCT calculation, the ZPE is not taken into account, which leads to the larger ICS of the QCT than of quantum calculation in the low energy range for such an exothermic reaction. In other words, in the low energy range, the quantum effect can be more apparent than in the high energy range. Also found in this figure is that the ICS decreases with increasing the collision energy, which is the common feature for an exothermic reaction. The decrease of the ICS with increasing collision energy may be caused by more repulsive areas on the PES opened at higher collision energy.[36] In this case, the increase of the collision energy will make it difficult for reactants to evolve into products following the MEP.

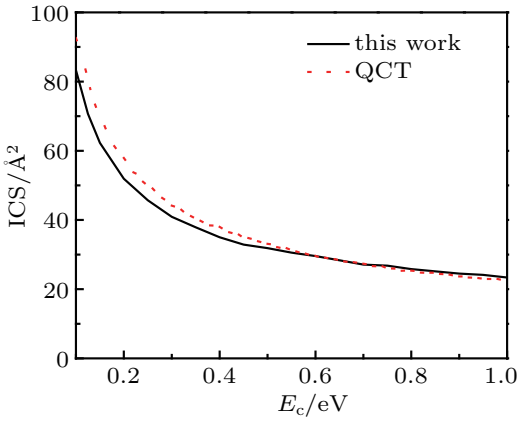


Fig. 5. Comparison of the present total ICSs with the previous QCT results.[21]

3.3. Product state distributions

The vibrational state-resolved ICSs of the reaction $S^+ + H_2(v = 0, j = 0) \rightarrow SH^+(v') + H$ are shown in Fig. 6. It is evident that the favorite formation state of the SH^+ product is the lower vibrational states, and the vibrational state-resolved ICSs do not present the quantum number inversion phenomenon. Besides, the formed SH^+ product states are ones with $v' \leqslant 3$ at low collision energy, and in contrast, the reactions with $v' > 3$ have reaction thresholds. This phenomenon can be explained by that for this exothermic reaction, the lower product vibrational states can be obtained through the internal energy conversion of intermediate complex, no need to apply the additional collision energy; but to obtain the higher product vibrational states, such as ones with $v' > 3$, only through providing a certain amount of collision energy, can the higher product vibrational states be obtained. Obviously, if the formed SH^+ product vibrational states are of above $v' = 3$, the reaction becomes endothermic.

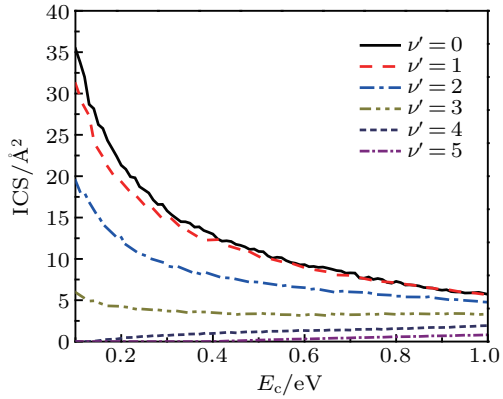


Fig. 6. Product vibrational state-resolved ICS changing with the collision energy for reaction $S^+ + H_2(v = 0, j = 0) \rightarrow SH^+(v') + H$.

Figure 7 displays the product rovibrational state distributions of the $S^+ + H_2$ reaction at five selected collision energies. As we can see from this figure, the rotational resolved ICSs exhibit also the obvious oscillating features. In addition, for this reaction system of heavy-light-light mass combination, the reactant orbital angular momentum can be easily transferred into the product rotation angular momentum,[37] we can deduce that the rotational excitation of the product is favorite for the reaction. Hence, we can find in this figure that the rotational quantum number of the SH^+ product under each vibrational state has a relatively wide range, and the quantum number inversion phenomenon occurs in the distribution of the product rotational states, just as shown in the bell-shaped distributions of the rotational states at five collision energies considered. In our previous work about the quantum state-to-state dynamics of $O^+ + H_2 \rightarrow OH^+ + H$,[31] we find that the maximum of ICS-j' distribution appears at about $j' = 10$ with the j' range of 0–25 for different collision energies, whereas for the present quantum state-to-state $S^+ + H_2 \rightarrow SH^+ + H$, the maxima of ICS-$j'$ distribution appear all at around $j' = 20$ with the j' range from 0–34 to 0–44 for different collision energies (v' is fixed at 0). Similar phenomenon can be observed in reaction $Cl + H_2 \rightarrow ClH + H$.[38] Although because of the energy conversion of the collision system, the number of the vibrational states of product SH^+ molecule increases with the increase of the collision energy, no vibrational inversion phenomenon occurs. Besides, it is noticed that this phenomenon becomes more pronounced as the collision energy increases from $E_c = 0.2$ eV to 1.0 eV, which can be rationalized by that with the increasing of the collision energy, more rotational channels of products are opened. But due to the reaction is exothermic with a potential well, the reaction becomes inhibited with the increase of collision energy, so the ICS decreases monotonously.

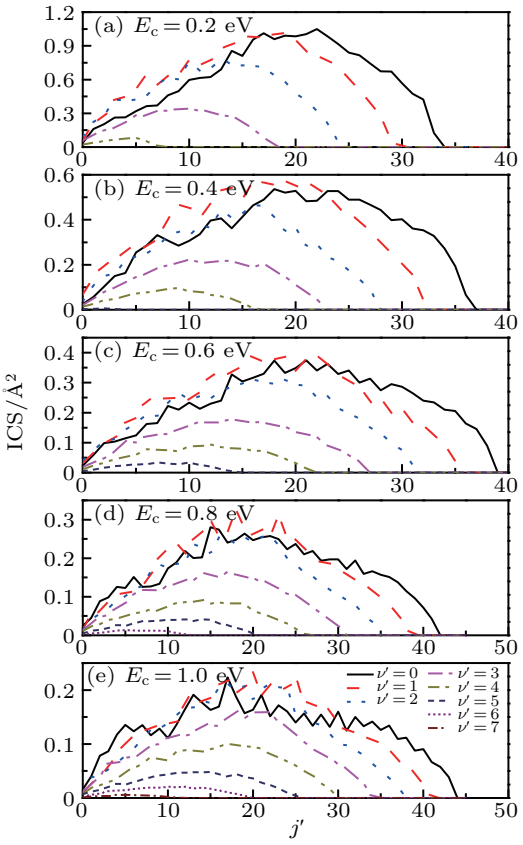


Fig. 7. Product rotational state distribution of $S^+ + H_2(v = 0, j = 0) \rightarrow SH^+(v', j') + H$ reaction at different collision energies.

3.4. DCSs

The total DCSs for reaction $S^+ + H_2 \rightarrow SH^+ + H$ at five selected collision energies are shown in Fig. 8. It is evident that the peak of the DCS is primarily in the forward and backward directions, and the DCSs have almost the forward and backward symmetric scattering distribution. The results show that there is a long-life complex formed in the reaction, which makes the reaction follow the statistical behavior, and the indirect reaction mechanism dominate in it. This complex completely loses the memory of the original direction of colliding particles, and the products are scattered randomly, not concen-

trated in one direction, but distributed symmetrically in the forward and backward directions. With the increasing of collision energy, the scattering intensity of most scattering angles has a tendency to decrease, being consistent with the ICS shown in Fig. 6.

To further describe the reaction in detail, we plotted the product state-resolved DCSs of reaction $S^+ + H_2(v = 0, j = 0) \rightarrow SH^+(v' = 0, 1, 2, j') + H$ as the function of ro-vibrational quantum number and scattering angle at two collision energies in Fig. 9. Obviously, the rotational distribution of the product is relatively wide, just as shown in Fig. 7. For the given total energy and translational energy, the vibrational energy and rotational energy of the product are negatively correlated. Besides, the product is mainly forward and backward scattering, which is consistent with that as shown in Fig. 8.

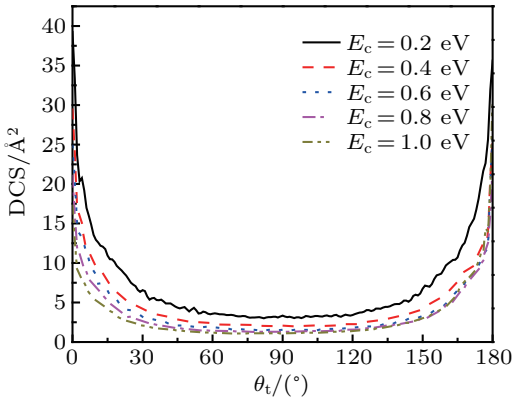


Fig. 8. Total DCSs of the title reaction as a function of scattering angles at five collision energies.

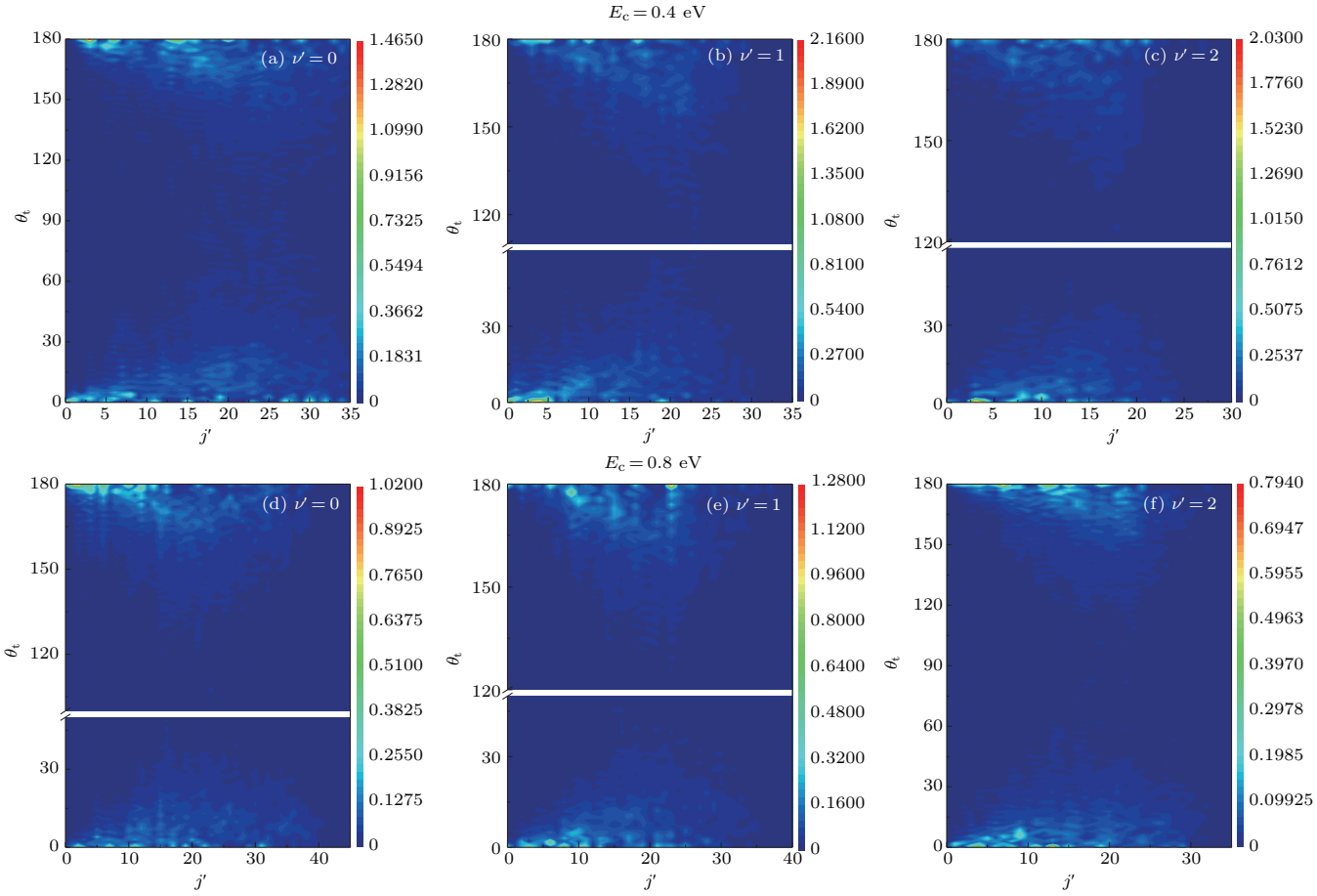


Fig. 9. Product state-resolved DCSs of $S^+ + H_2(v = 0, j = 0) \rightarrow SH^+(v', j') + H$ reaction at two selected collision energies.

4. Conclusion and perspectives

In this work, we have investigated the state-to-state reaction dynamics of $S^+(^2D) + H_2(X^1\Sigma_g^+) \rightarrow SH^+(X^3\Sigma^-) + H(^2S)$ on an accurate X^2A'' PES based on the GPU version of TDWP code. The reaction probabilities, total and state-resolved ICSs and DCSs were studied and the total ICSs are in good agreement with the QCT result. Due to the existence of the potential well, there are a large number of oscillating structures in the reaction probability, ICS and DCS. The nature of the oscillation can be attributed to the indirect mechanism. Besides, increasing the collision energy can lead to the decrease of reaction probability and ICS, which is the common feature of exothermic reactions. In contrast to no quantum number inversion in the vibrational distribution, the rotational resolved ICSs have an obvious inversion phenomenon. The product DCSs, total or state-resolved, are all mainly with the characteristics of the forward and backward scattering. The results also show that the existence of the long-life complex

makes the reaction follow the statistical behavior.

References

[1] Farquhar J, Bao H and Thiemens M H 2000 *Science* **289** 756
[2] Habicht K S, Gade M, Thamdrup B, Berg P and Canfield D E 2002 *Science* **298** 2372
[3] Martínez R, Millán J and González M 2004 *J. Chem. Phys.* **120** 4705
[4] Smith D, Adams N G and Lindinger W 1981 *J. Chem. Phys.* **75** 3365
[5] Stowe G F, Schultz R H, Wight C A and Armentrout P 1990 *Int. J. Mass Spectrom. Ion Processes* **100** 177
[6] Duxbury G, Jungen C, Alijah A, Maier J and Klapstein D 2014 *Mol. Phys.* **112** 3072
[7] Horani M, Leach S and Rostas J 1967 *J. Mol. Spectrosc.* **23** 115
[8] Dixon R, Duxbury G, Horani M and Rostas J 1971 *Mol. Phys.* **22** 977
[9] Duxbury G, Horani M and Rostas J 1972 *Proc. R. Soc.*, 21 November, 1972
[10] Delwiche J and Natalis P 1970 *Chem. Phys. Lett.* **5** 564
[11] Han S, Kang T Y and Kim S K 2010 *J. Chem. Phys.* **132** 124304
[12] Sakai H, Yamabe S, Yamabe T, Fukui K and Kato H 1974 *Chem. Phys. Lett.* **25** 541
[13] Bruna P J, Hirsch G, Perić M, Peyerimhoff S D and Buenker R J 1980 *Mol. Phys.* **40** 521
[14] Lahmar S, Lakhdar Z B, Chambaud G and Rosmus P 1995 *J. Mol. Struct.: THEOCHEM* **333** 29
[15] Takeshita K and Shida N 1996 *Chem. Phys.* **210** 461
[16] Hirst D M 2003 *J. Chem. Phys.* **118** 9175
[17] Li W Z and Huang M B 2005 *Chem. Phys.* **315** 133
[18] Chang H B and Huang M B 2009 *Theor. Chem. Acc.* **122** 189
[19] Zanchet A, Agúndez M, Herrero V J, Aguado A and Roncero O 2003 *Astrophys. J.* **146** 125
[20] Song Y Z, Zhang Y, Gao S B, Meng Q T, Wang C K and Ballester M Y 2018 *Mol. Phys.* **116** 129
[21] Zhang L L, Gao S B, Meng Q T, Pan J and Song Y Z 2018 *J. Chem. Phys.* **149** 154303
[22] Bulut N, Castillo J F, Jambrina P G, Klos J, Roncero O, Aoiz F J and Banares L 2015 *J. Phys. Chem. A* **119** 11951
[23] Zhang P Y and Han K L 2013 *J. Phys. Chem. A* **117** 8512
[24] Zhang P Y and Han K L 2014 *J. Phys. Chem. A* **118** 8929
[25] Zhang P Y and Han K L 2015 *Int. J. Quantum Chem.* **115** 738
[26] Zhang J, Gao S B, Wu H and Meng Q T 2015 *J. Phys. Chem. A* **119** 8959
[27] Wu H, Yao C X, He X H and Zhang P Y 2016 *J. Chem. Phys.* **144** 184301
[28] Zhang J, Gao S B, Wu H and Meng Q T 2015 *Chin. Phys. B* **24** 083104
[29] Xu T, Zhao J, Wang X L and Meng Q T 2019 *Chin. Phys. B* **28** 023102
[30] Xu T, Wu H, Zhang L L, Wang X L, Zhao J and Meng Q T 2019 *Mol. Phys.* **117** 311
[31] Xu T, Zhang J, Zhao J, Song Y and Meng Q 2019 *Europhys. Lett.* **126** 53001
[32] Zhao J, Wu H, Sun H B and Wang L F 2018 *Chin. Phys. B* **27** 023102
[33] Li Y Q, Zhang P Y and Han K L 2015 *J. Chem. Phys.* **142** 124302
[34] Ma H Y, Guo Q and Li Y Q 2019 *Spectrochim. Acta Part. A* **219** 267
[35] Zhang John Z H 1998 *Theory and application of quantum molecular dynamics* (Singapore: World Scientific)
[36] Duan Z X, Li W L, Xu W W and Lv S J 2013 *J. Chem. Phys.* **139** 094307
[37] Zhao J, Xu T, Zhang L L and Wang L F 2020 *Chin. Phys. B* **29** 023105
[38] Balakrishnan N 2012 *J. Chem. Sci.* **124** 311